J Mater Sci (2010) 45:1328–1335
DOI 10.1007/s10853-009-4086-3

Isothermal crystallization kinetics of poly(vinylidene fluoride) in the α-phase in the scope of the Avrami equation

V. Sencadas · C. M. Costa · J. L. Gómez Ribelles · S. Lanceros-Mendez

Received: 20 September 2009 / Accepted: 25 November 2009 / Published online: 9 December 2009

Abstract Isothermal melt crystallization of poly(vinylidene fluoride) (PVDF) at different crystallization temperatures was studied by differential scanning calorimetry. Analysis by the two different approaches of the Avrami equation was performed: first the classical double logarithmic approximation was used, but a non-linear least squares search showed to clearly improve the fit of the model to the experimental isotherms. The differences found by both methods in the Avrami parameters are discussed. The limitation of the Avrami equation in this polymer has to do not only with the fitting procedure to determine the parameters but also with the lack of a consistent physical interpretation of their temperature evolution. The melting behavior of the samples was analyzed and an equilibrium melting temperature of 190.9 °C was obtained by the Hoffmann–Weeks extrapolation. The samples crystallize in a spherulitic structure, as observed by optical microscopy with polarized light (OMPL). Lauritzen–Hoffmann theory was applied to analyze the crystallization kinetics and the Regime III was found for the crystallization of α-PVDF.

V. Sencadas · C. M. Costa · S. Lanceros-Mendez (✉)
Departmento de Física, Universidade do Minho, Campus de Gualtar, 4710-057 Braga, Portugal
e-mail: lanceros@fisica.uminho.pt

C. M. Costa
CeNTI - Centre for Nanotechnology and Smart Materials, Rua Fernando Mesquita 2785, 4760-034 Vila Nova de Famalicão, Portugal

V. Sencadas · J. L. Gómez Ribelles
Centro de Biomateriales, Universidad Politécnica de Valencia, 46022 Valencia, Spain

J. L. Gómez Ribelles
Regenerative Medicine Unit, Centro de Investigación Príncipe Felipe, Autopista del Saler 16, 46013 Valencia, Spain

J. L. Gómez Ribelles
CIBER en Bioingeniería, Biomateriales y Nanomedicina, Valencia, Spain

Introduction

Poly(vinylidene fluoride) (PVDF) is known for its remarkable electrical, mechanical, and chemical properties, leading to electro-optical, electromechanical, and biomedical applications [1]. In particular, PVDF is being widely investigated due to its outstanding pyro- and piezoelectric properties among polymer systems [1]. The existence and optimization of these properties are intimately related with the morphology and crystallinity of the polymer, which in turn depend on the crystallization of the polymer and therefore on the processing conditions [2–4].

PVDF is also known for its unusual polymorphism: It shows four crystalline phases named: α, β, δ, and γ. Upon cooling from melt at rapid or moderated rate, the apolar α-phase is obtained. When the crystallization is performed at crystallization temperatures above 155 °C and for longer crystallization times, the material crystallizes in two coexisting phases: α and γ-PVDF. The presence of γ-PVDF in the sample increases with increasing crystallization temperature [1, 4]. Electroactive β-PVDF can be obtained by mechanical stretching of the α-phase films at suitable temperatures [4–6]. δ-PVDF is obtained applying an electric field of several kilovolts to α-PVDF [1, 3].

The crystallization behavior of PVDF and blends based on PVDF was widely investigated [7–9]. Liu et al. [7] studied the crystallization and morphology behavior of PVDF/polyhydroxybutyrate blends, they depicted a phase

diagram for these blends based on calorimetric measurements. They report that the Avrami exponent for pure PVDF is approximately 3 when the Avrami conditions are fulfilled. It is suggested that the growth of spherulites is three-dimensional with athermal-induced quench nucleation. They also reported that the half crystallization time ($t_{1/2}$) of PVDF increases with increasing crystallization temperature.

The miscibility of PVDF/poly(butylene sucinate-*co*-adipate) was studied by Liu et al. [8]. These authors report that the crystallization of PVDF is affected by the crystallization temperature and the average values of the Avrami exponent are around 2.5, indicating that the crystallization of PVDF might correspond to the spherulitic growth with heterogeneous nucleation.

Chui [9] studied the spherulitic morphology and crystallization kinetics of PVDF/polyvinyl alcohol blends. This author found an Avrami exponent of approximately 3 for PVDF and suggests that the crystallization of the polymer occurs in a spherulitic growth with heterogeneous nucleation. Mancarella and Martuscelli [10] investigated the crystallization behavior of PVDF, reporting that the Avrami exponent varies between 2.99 and 4.60 and the half crystallization time increases with increasing crystallization temperature. As observed, there are significant variations among the Avrami values found in the literature.

The electroactive properties of PVDF are intimately related with the phase content, morphology, and crystallinity of the polymer material, which in turn depend on the processing conditions. The solid-state α to β-phase transformation is dependent on the microstructure of the α-phase, which deeply influences the electroactive properties of the β-PVDF. Furthermore, in order to prepare composites based in this material it is essential to characterize and understand the crystallization of the matrix.

This study reports on the kinetics of the isothermal melt crystallization and spherulitic morphology of α-PVDF at different crystallization temperatures by differential scanning calorimetry. Avrami theory was applied in two different approaches to analyze the crystallization kinetics and discuss the validity of the Avrami approach for this material. Hoffmann–Weeks (HW) extrapolation was applied and the value of the equilibrium melting temperature was calculated. The Lauritzen–Hoffmann (LH) approach was also employed to estimate the kinetics parameters.

Experimental methods

Sample preparation

PVDF samples were prepared by spreading a solution of the polymer resin (Solef 1100 from Solvay, Bollate, Italy) in *N*,*N*-dimethyl formamide (MERCK, Darmstadt, Germany) on a glass slide. The initial concentration of the solution was 20% (w/w) of PVDF. The system was kept inside an oven at 120 °C during 60 min. This time was enough to insure the removal of all solvent by evaporation. After evaporation of the solvent, the sample was melted at 220 °C for 10 min, removed from the oven, and cooled down at room temperature. After this procedure, the crystalline phase present in the polymer is α-PVDF [4].

Crystallization kinetics measurements

Crystallization kinetics of PVDF was measured by means of isothermal experiments and cooling scans using a differential scanning calorimeter (DSC) Pyris (Perkin-Elmer, Waltham, MA, USA). Dry nitrogen gas was let through the DSC cell with a flow rate of 20 mL min^{-1}. A single sample of about 4 mg directly cut from the film was used for all isothermal experiments. The calibration of the DSC for cooling scans was made using the 4-cyano-4′-octyloxybiphenyl (M24) transition from smectic to nematic phase, T_{s-n}, measured at different temperature rates on cooling and heating runs and the melting point of indium measured at different heating rates. The measurements were conducted with the standard calibration of the DSC and the temperature scale was then corrected by software taking into account the rate dependence of T_{s-n} and the indium melting.

Images of spherulitic growth during the crystallization of PVDF were obtained by an OMPL (Olympus BH-2). Snapshots were taken using a Leica DFC-280 camera.

Results and discussion

Spherulitic morphology

The morphology of the semi-crystalline polymers was observed by OMPL. Figure 1 shows the spherulitic morphology of PVDF crystallized at different isothermal temperatures from 140 to 160 °C.

Spherulites of PVDF display compact and well-defined *Maltese-cross* texture as shown in Fig. 1. The material crystallized at the lowest temperature shows the finest spherulitic microstructure. The diameter of the spherulites increases with increasing crystallization temperature (Fig. 1).

Overall crystallization kinetics

Typical DSC thermograms of PVDF crystallized at different temperatures are presented in Fig. 2. It is observed that the crystallization exothermic peak shifts to larger times and peak width increases with increasing

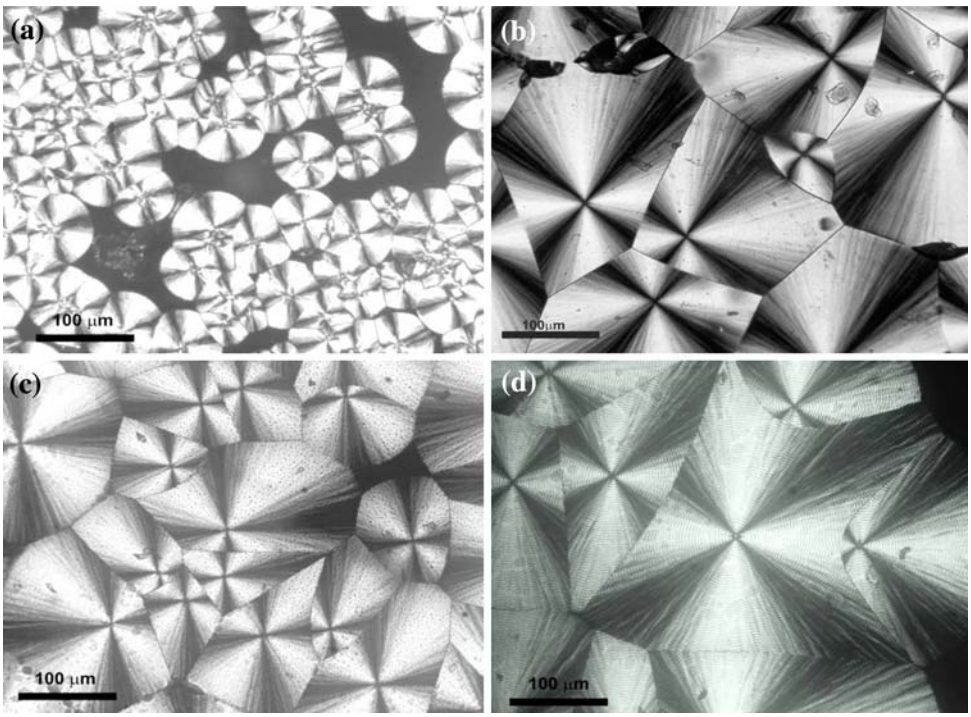

Fig. 1 Spherulite structure of PVDF samples crystallized at: **a** 150 °C, **b** 155 °C, and **c** 160 °C, **d** 165°C. Image **a** was taken during the crystallization process; **b–d** with a fully crystallized sample

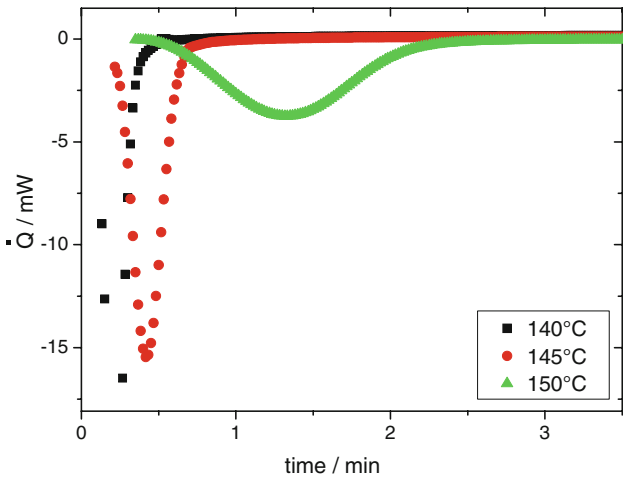

Fig. 2 Crystallization exotherms for PVDF at different temperatures

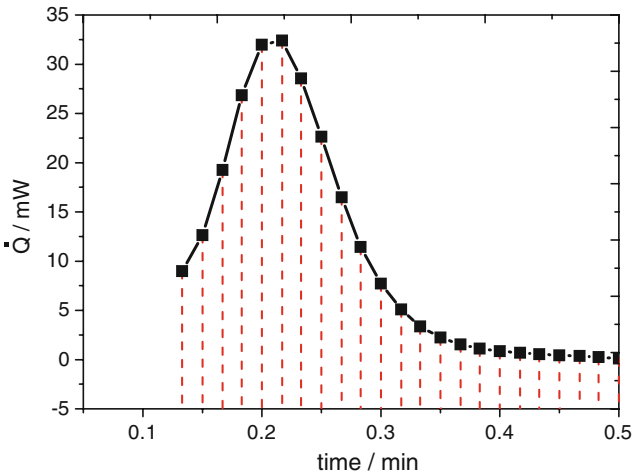

Fig. 3 Crystallization exotherm for α-PVDF at 140 °C

crystallization temperature (T_c). This fact is due to decreasing crystallization rate with increasing T_c. The bell shape of the peaks suggests a primary crystallization with no obvious secondary crystallization occurring at later stages of isothermal crystallization process. Furthermore, it can be observed that the crystallization isotherms present the characteristic sigmoid shape.

The overall crystallization kinetics is determined by the nucleation and growth rates. The study of crystallization kinetics can be carried out by DSC. Figure 3 shows the crystallization exotherm for PVDF at 140 °C.

The relative degree of crystallinity (X_t) present at a given time t can be calculated by:

$$X_t = \frac{\int_0^t \left(\frac{\partial H}{\partial t}\right)\partial t}{\int_0^\infty \frac{\partial H}{\partial t}\partial t} \quad (1)$$

where $(\partial H/\partial t)$ is the DSC heat flow. The numerator represents the area of isotherms at a given time t and the denominator is the total exothermal area. Now, the Avrami equation [11–13] can be applied:

$$1 - X_t = \exp(-kt^n) \quad (2)$$

where k is the overall crystallization rate constant containing contributions from both nucleation and growth rate, and n is the Avrami exponent which depends on the nature of the nucleation and growth geometry of the crystals [11–13]. The plot of

$$\ln[-\ln(1-X_t)] = n\ln t + \ln k \quad (3)$$

represents a linear behavior from which the parameters k and n can be obtained from the intercept and slope, respectively. Typically, the Avrami equation represents correctly just the initial steps of polymer crystallization (initial linear region). The spherulites grow outward with a constant radial growth rate until impingement takes place when they stop growing at the intersection. Then a secondary crystallization process is often observed after the initial spherulite growth in the amorphous interstices [9]. Equation 3 is valid only if the nucleation and growth conditions do not change during the crystallization process.

Figure 4 shows the evolution of the relative degree of crystallinity (X_t) with time t for the various crystallizations temperatures. The initial slope of the isotherms decreases with increasing isothermal crystallization temperature, indicating a progressively slower crystallization rate.

The kinetics of the overall crystallization of PVDF was further analyzed on the basis of the pure Avrami model (Eq. 3). Figure 5 shows the Avrami plots of PVDF at various T_c. The experimental data closely agree with the Avrami equation in the initial steps. From the slopes of the fitted data (Fig. 5) the n and k values were estimated (Table 1).

Further, the half-time crystallization ($t_{1/2}$) defined as the time required to reach half of the final crystallinity can be calculated from k

$$t_{1/2} = \left(\frac{\ln 2}{k}\right)^{1/n} \quad (4)$$

Reciprocal half-time crystallization ($1/t_{1/2}$) can be considered approximately proportional to the crystallization growth rate (G) [14] (Fig. 6). Figure 7 shows the temperature dependence of $1/t_{1/2}$ that corresponds to the right side of typical bell-shaped curve for the polymer crystallization kinetics that occurs between the glass transition and the melting temperature.

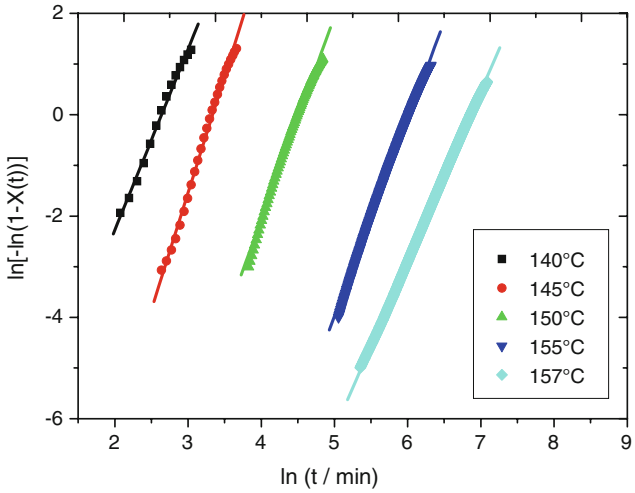

Fig. 5 Avrami plots for α-PVDF at various crystallization temperatures

Table 1 Overall crystallization data based on the general Avrami equation

T_c (°C)	n	k (min^{-1})	$t_{1/2}$ (min)
140	3.64	6.84E−05	0.21
142.5	4.16	3.96E−06	0.30
145	4.49	3.09E−07	0.43
147.5	4.54	2.41E−08	0.73
150	4.60	1.00E−09	1.39
152.5	4.32	1.50E−10	2.88
155	4.01	3.38E−11	6.21
157.5	3.30	1.43E−10	14.36

The values of n, k, and $t_{1/2}$ for each crystallization temperature are reported in Table 1. To check the quality of the classical linear fit obtained with Eq. 3, the heat flow emitted per unit sample mass was calculated from Eq. 1 as:

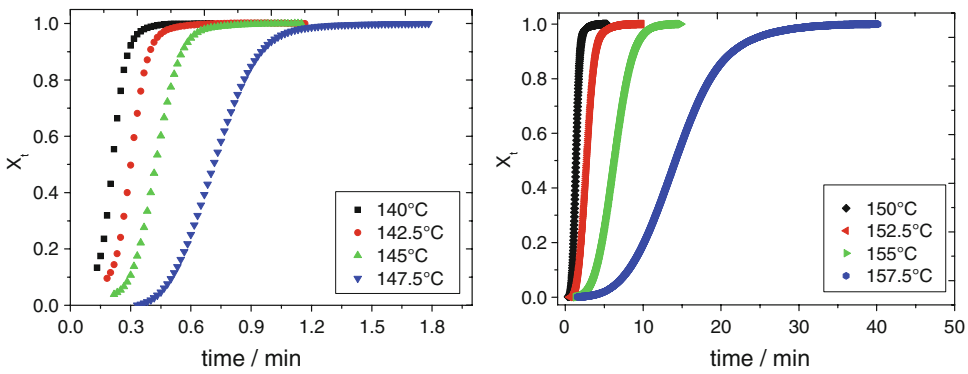

Fig. 4 Evolution of the relative degree of crystallinity with time for α-PVDF crystallized at different temperatures

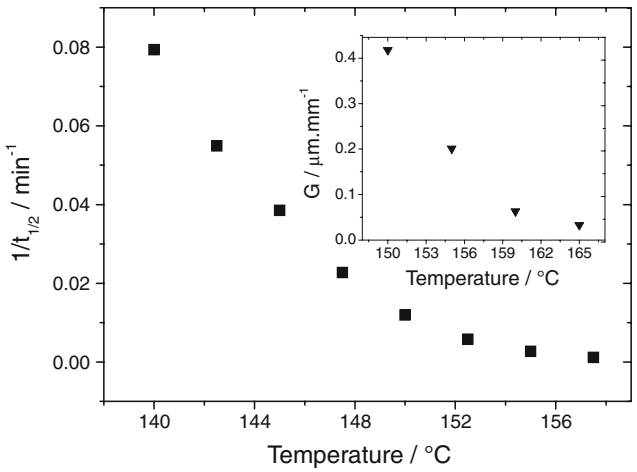

Fig. 6 Reciprocal half-time of crystallization as a function of the crystallization temperature for PVDF. *Inset*: Spherulitic growth rate

$$\dot{q}(t) = \phi_c^{\infty}\frac{\rho_c}{\rho}\Delta H_F\frac{dX_t}{dt} \quad (5)$$

where ρ_c and ρ are the density of the crystal phase and the whole sample, respectively, ϕ_c^{∞} the maximum volume fraction of the crystal phase obtained in the isothermal crystallization process and ΔH_F the melting enthalpy. The curves calculated by Eqs. 2 and 5 and the parameters of Table 1 are compared with the experimental thermograms in Fig. 7 for two experimental temperatures. It can be observed from Fig. 7 that for the 150 °C isotherm, the maximum of the curve predicted by the model equation is shifted toward longer times, whereas at 145 °C the exothermal peak calculated is broader than the experimental. The fit can be improved using a non-linear direct least-squares search routine of each isotherm to give the value of the exponent n and $k(T)$. As shown in Fig. 7, the fit clearly improves (black lines in Fig. 7) but the Avrami coefficient varies significantly, as shown in Fig. 8 and Table 1. Significant variations are also observed for $k(T)$. On the other hand, the half-time crystallization ($t_{1/2}$) calculated by Eq. 4 is indistinguishable when calculated by both approaches.

The evolution of the Avrami fitting parameters for the two different approaches is represented in Fig. 8 for comparison.

So, it is demonstrated that the Avrami fitting parameters and their behavior are different depending on the fitting procedure. Using the linear fitting of Eq. 3, the Avrami exponent of the material shows a bell shape with maximum at 150 °C. The n parameter has an average value approximately 4 which suggests that the crystallization occurs in a spherulite growth with thermal quenched-induced nucleation in a tridimensional mode. The same results were observed by Mancarella and Martuscelli [10] and are in agreement with the optical observations (Fig. 1). On the other hand, the more accurate non-linear fitting provided by Eq. 5 shows that n decreases from approximately 5 to 3 with increasing crystallization temperature.

This fact is quite surprising as the coefficient 3, corresponding to athermal nucleation, is most likely to occur at low temperatures, when nucleation velocity is larger. Athermal nucleation is characterized by the fact that all crystallization nuclei are already formed when the crystallization process begin. This fact is detected by the existence of a large number of similar size small spherulites, all of them starting to grow at the same time. This is in fact what is observed in Fig. 1a. On the other hand, at

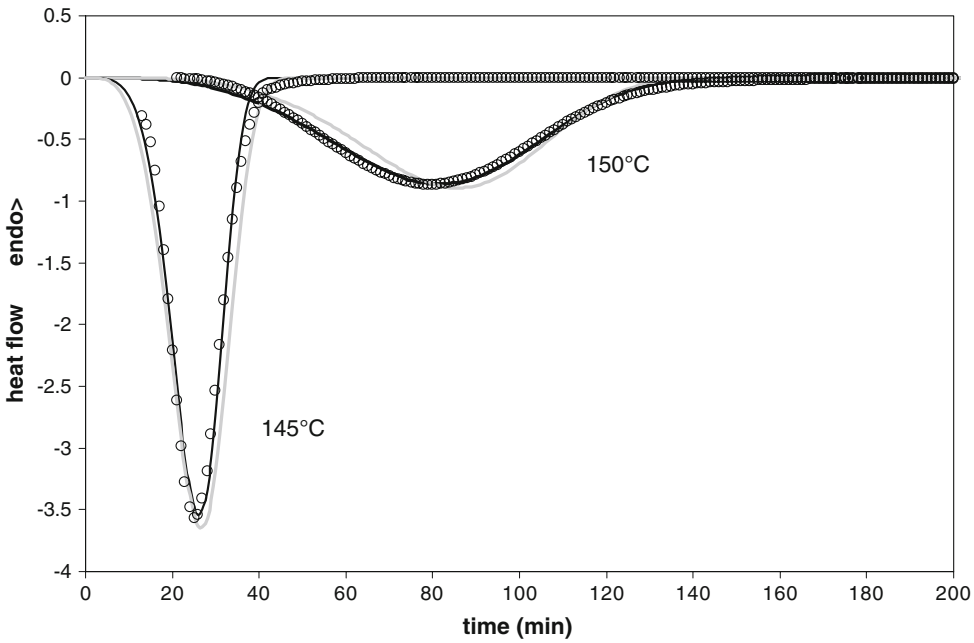

Fig. 7 Comparison of the fit with the Avrami equation to the experimental 145 and 150 °C isotherms using the linear fit given by Eq. 3 (*grey lines*) and the non-linear least squares fit to the experimental thermogram (*black lines*). Only two isotherms are represented for the sake of clarity, the fitting in the case of the other isotherms is similar

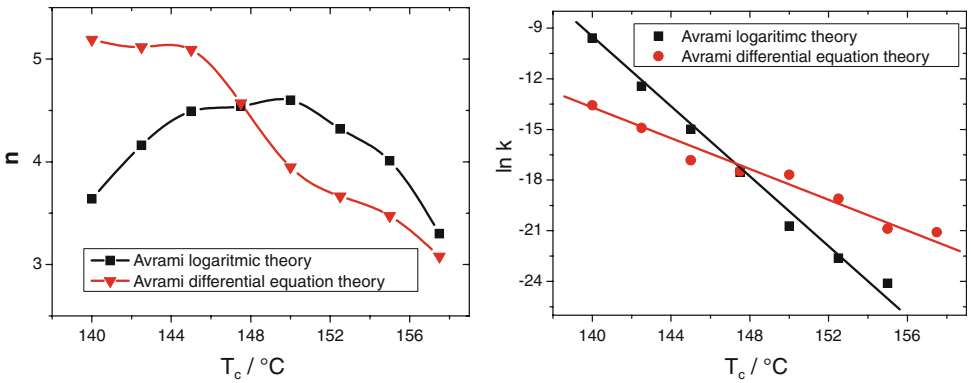

Fig. 8 Comparison of the Avrami fitting parameters: Avrami exponent, n (*left*) and overall crystallization rate, k (*right*)

high temperatures and with low nucleation rates, a lower number of spherulites are detected. The nuclei are formed along the time, so the spherulites show different sizes and the spherulite intersections are curved. These facts are detected in Fig. 1d. The apparent contradiction between the fitting results for the exponents in Fig. 9 and the spherulite morphology of Fig. 1 clearly indicates the limitations of the physical basis of the Avrami model, as already discussed in [15]. The model is appropriate to reproduce the sigmoidal behavior of Fig. 3 but lacks a straightforward and clear physical basis.

Figure 1 shows in fact that the material crystallizes in a spherulite growth (for lower T_c) with athermal nucleation and with increasing crystallization temperature the polymer changes regime crystallization in a spherulitic growth but with thermal nucleation.

The overall crystallization rate, k, also shows different behavior for the two fitting procedures. The slopes of the straight lines show different values, being −0.995 for the model of Eq. 1 and approximately a half (−0.426) of the differential equation approach.

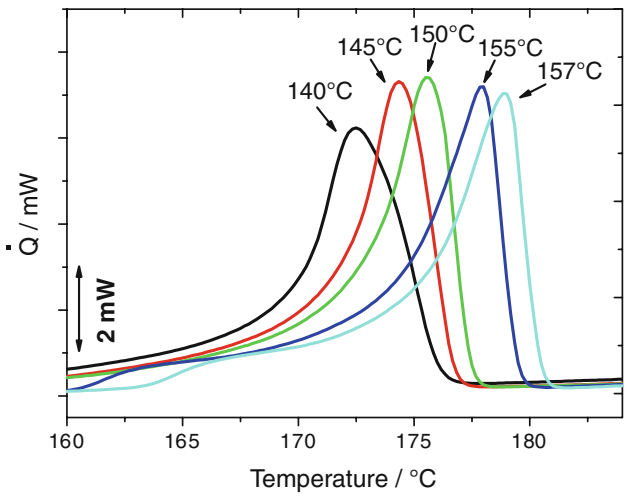

Fig. 9 DSC thermograms of PVDF crystallized at different temperatures

In order to determine the equilibrium melting temperature $\left(T_m^0\right)$ of the polymer, melting points of the PVDF samples (Fig. 9) were measured by DSC scans from 50 to 220 °C, after isothermal crystallization. Figure 10 shows the melting temperature (T_m) of PVDF versus crystallization temperature (T_c) (HW plot [16]) and extrapolated to $T_m = T_c$ by linear HW extrapolation:

$$T_m = \frac{T_c}{\gamma} + T_m^0\left(1 - \frac{1}{\gamma}\right) \tag{6}$$

where γ is the thickening ratio [16].

The value of T_m^0 obtained was 190.9 °C, which is coherent with the values reported in literature. Briber and Khoury [17] found a T_m^0 value for PVDF of 184 °C, Morra and Stein [18] reported a value of 201 °C, and Mancarella and Martuscelli [10] present a T_m^0 value in the range between 178 and 210 °C, being the later temperature near the estimated Curie transition temperature of PVDF (208–210 °C) [19].

It was previously pointed [18] that the differences in T_m^0 appear to depend on head-to-head defect content of the polymer. This explanation was supported by the observation of a change in the slope on the HW plot occurring at

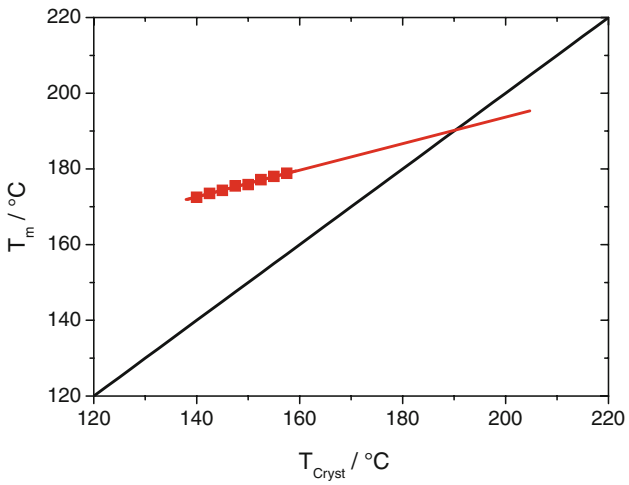

Fig. 10 HW extrapolation plot for the α-PVDF

about 160 °C with the value of T_m^0 obtained from crystallization data above 160 °C being about 25 °C higher than that obtained from crystallization data below 160 °C. In our opinion, the differences of the crystallization temperatures found by Morra and Stein [18] are not due to head-to-head defect content of the polymer but just explained by the presence of γ-PVDF on the samples that crystallize at temperatures above 160 °C, as this polymorph of PVDF has a melting temperature higher than the α-phase [1, 4, 20]. At temperatures above 160 °C, two phases of PVDF (α and γ-phase) crystallize simultaneously with different crystallization kinetics and thermal behavior [20].

In the HW linear analysis, the thickening ratio must be in the range between 2 and 3 [16]. The value of 2.77 was found for the γ value of α-PVDF.

In the case of a spherulitic growth with chain-folded lamellae where a two-dimensional surface nucleation process controls the radial growth of spherulites, then the overall crystallization rate k can be expressed, according to the HW kinetic theory, by the following equation [10]:

$$\text{Log } k = A_0 - \frac{\Delta F^*}{2.3kT_c} - \frac{4b_0\sigma\sigma_e T_m^0}{2.3k\Delta H_F T_c \Delta T} \quad (7)$$

where A_0 is a constant, which means that the spherulite nucleus density is independent of time, melting temperature, and crystallization temperature [21]. ΔF^* is the activation energy for the transport process across the liquid–crystal interface, k the Boltzmann constant, b_0 the distance between adjacent fold planes, ΔH_F the enthalpy of fusion and $\Delta T\left(\Delta T = T_m^0 - T_c\right)$ the undercooling, and σ_e and σ are the surface-free energy per unit area, perpendicular and parallel, respectively.

Figure 11 represents the ln k versus $T_m^0/T_c\Delta T$ plot for the equilibrium melting temperature 190.9 °C.

According to Eq. 7, this result shows that at least in the vicinity of the melting point and for the values of the undercooling used in this study, the transport term $\frac{\Delta F^*}{2.3kT_c}$ may be considered as a constant. From the slope of the straight line, the quantity $\frac{4b_0\sigma\sigma_e T_m^0}{2.3k\Delta H_F}$ is estimated to be 355.1 K for T_m^0.

The free energy of formation for a nucleus of critical dimensions ΔΦ can be calculated by the following equation:

$$\Delta\Phi = \frac{4b_0\sigma\sigma_e T_m^0}{\Delta H_F \Delta T} \quad (8)$$

The dependence of the ΔΦ upon the undercooling is presented in Fig. 12 for $T_m^0 = 190.9$ °C.

According to the crystallographic data of the α-PVDF of Lando et al. [22], the most probable fold planes are the (200) and then the distance of two adjacent fold planes b_0 is estimated to be 4.83 Å. The fusion enthalpy of the α-phase is 2.01×10^9 erg cm^{-3} [23]. The quantity $\sigma\sigma_e$ may be

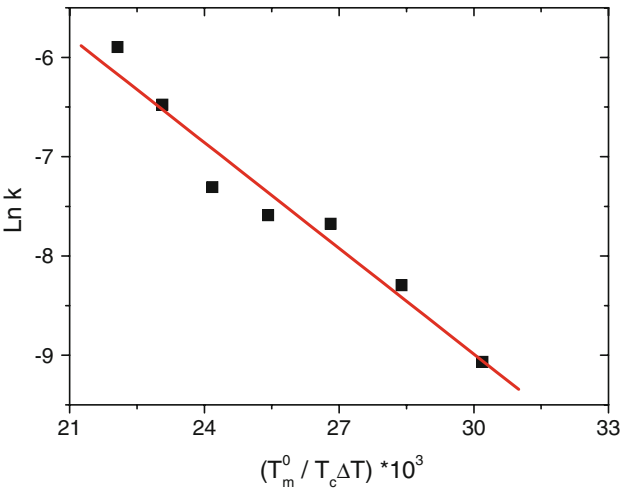

Fig. 11 Plot of ln k versus $T_m^0/T_c\Delta T$

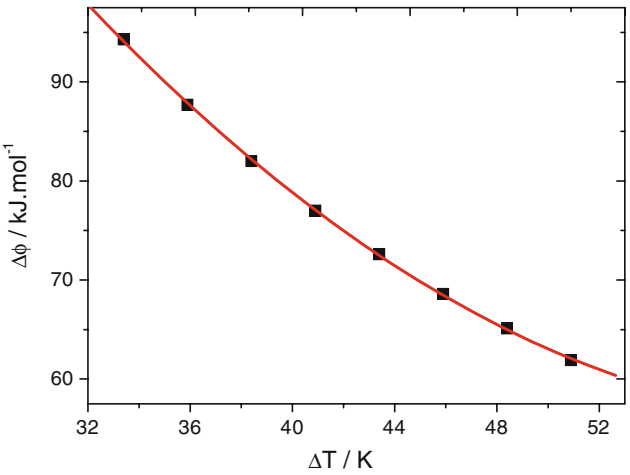

Fig. 12 Variation of ΔΦ with the undercooling ΔT

calculated by substituting the values of b_0 and ΔH_F in the term $\frac{4b_0\sigma\sigma_e T_m^0}{2.3k\Delta H_F}$. The value found for $\sigma\sigma_e$ was 1.17×10^{-3} J m^{-4}.

From Eq. 9:

$$\sigma = \alpha\Delta H_F b_0 \quad (9)$$

where α is equal to 0.1 for all polymers, the surface-free energy parallel to the chain direction σ is estimated to be 9.71×10^{-3} J m^{-2}. Then the surface-free energy of folding σ_e was calculated and a value of 1.21×10^{-01} J m^{-2} was found. The values found for the σ_e and σ are in good agreement with the ones obtained by Mancarella and Martuscelli [10].

The average of lamellar thickness l^* can be evaluated by applying the LH theory [24] to the experimental data. The average of the initial lamellar thickness observed at T_{cryst} can be expressed by

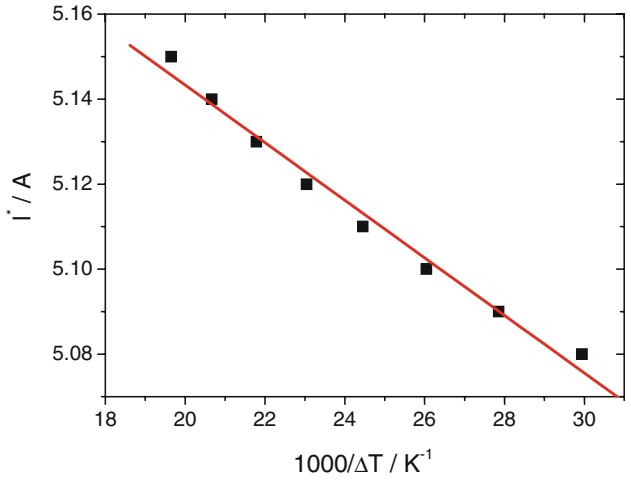

Fig. 13 Evolution of l^* with the undercooling temperature ΔT

Table 2 Summary of the physical parameters obtained by the application of the HW and LH approaches to α-PVDF

T_m^0 (°C)	γ	δl (Å)	$\sigma\sigma_e$ (J^2 m^{-4})	σ (J m^{-2})	σ_e (J m^{-2})
190.9	2.77	5.27	1.17×10^{-3}	9.71×10^{-3}	1.21×10^{-1}

Here, T_m^0 is the equilibrium melting temperature, γ represents the thickening ratio, δl is the thickness increment above the minimum lamellar thickness, σ the surface-free energy parallel to the chain direction surface-free energy of folding σ_e

$$l^* = \frac{2\sigma_e T_m^0}{\Delta H_F\left(T_m^0 - T_{cryst}\right)} + \delta l \frac{2\sigma_e T_m^0}{\Delta H_F\left(T_m^0 - T_m\right)} \quad (10)$$

where δl is the thickness increment above the minimum lamellar thickness. A thickness increase of 5.27 Å was found. Figure 13 shows the evolution of the average lamellar thickness with the undercooling ΔT.

Table 2 shows the different parameters calculated by the HW and by the LH theory for α-PVDF.

Conclusions

The kinetics of crystallization of the α crystalline phase of PVDF was characterized by means of isothermal DSC experiments. Avrami equation was applied using the usual linearization given by Eq. 3. Nevertheless, the fit obtained with this procedure can be significantly improved by means of non-linear least squares fit of the DSC thermograms, using Eq. 5. The temperature dependence of the model parameters changes significantly due to the different statistical weight of different parts of the curve in the double logarithmic expression. In the temperature range in which the experiments could be performed, the crystallization rate diminishes as temperature increases, thus all the isotherms are above the temperature of the maximum crystallization rate. Crystallization at lower temperatures in the DSC starts with a significant initial crystalline phase formed during cooling. The physical interpretation of the parameters is not straightforward. Optical microscopy shows that the PVDF have a spherulite morphology.

The values of the equilibrium melting temperature $T_m^0 = 190.9$ °C was estimated based on the linear HW extrapolation. Using this melting equilibrium temperature, the $\sigma\sigma_e$ value is 1.17×10^{-3} J^2 m^{-4}, whereas σ is 9.71×10^{-3} J m^{-2}. At the crystallization temperatures studied in this study, α-PVDF crystallizes in the regime III of the LH theory.

Acknowledgements The authors thank the COST action 12 "Structuring Polymers" and the Portuguese Foundation for Science and Technology (FCT) for financial support (Grants POCI/CTM/59425/2004, PTDC/CTM/69362/2006, and SFRH/BD/16543/2004 to V.S.). J.L.G.R. acknowledges the support of the Spanish Ministry of Science through Project No. MAT2007-66759-C03-01. The authors also thank to Solvay for providing the excellent quality material.

References

1. Lovinger AJ (1982) In: Basset DC (ed) Developments in crystalline polymers, vol 1. Elsevier Applied Science, London
2. Sencadas V, Moreira VM, Lanceros-Mendez S, Pouzada AS, Gregorio R Jr (2006) Mater Sci Forum 514:872
3. Nalwa HS (1995) Ferroelectric polymers: chemistry, physics, and applications, vol 1. Marcel Dekker, Inc., New York
4. Sencadas V, Lanceros-Mendez S, Gregorio R Jr (2009) J Macromol Sci B Phys 48:514
5. Gregorio R Jr, Ueno EM (1999) J Mater Sci 34:4489. doi: 10.1023/A:1004689205706
6. Matsushige K, Nagata K, Imada S, Takemura T (1980) Polymer 21:1391
7. Liu J, Qiu Z, Jungnickel BJ (2005) J Polym Sci B Polym Phys 43:287
8. Liu J, Yan C, Lu J, Yang W (2007) Macromolecules 40:5047
9. Chiu H-J (2002) J Polym Res 9:169
10. Mancarella C, Martuscelli E (1977) Polymer 18:1240
11. Avrami M (1939) J Chem Phys 7:1103
12. Avrami M (1940) J Chem Phys 8:212
13. Avrami M (1941) J Chem Phys 9:177
14. Iannace S, Nicolais L (1997) J Appl Polym Sci 64:911
15. Strobl GR (1997) Physics of polymers: concepts for understanding their structures and behavior. Springer, Berlin
16. Hoffman JD, Weeks JJ (1962) J Res Natl Bur Stand 66:13
17. Brider RM, Khoury F (1987) Polymer 28:38
18. Morra BS, Stein RS (1982) J Polym Sci Polym Phys 20:2261
19. Ducharme S, Bune AV, Blinov LM, Fridkin VM, Palto SP, Sorokin AV, Yudin SG (1998) Phys Rev B 57:25
20. Silva MP, Sencadas V, Rolo AG, Botelho G, Machado AV, Rocha JG, Lanceros-Méndez S (2008) Mater Sci Forum 587–588:534
21. Godowsky YK, Slonimisky JG (1974) J Polym Sci Polym Phys 12:1053
22. Lando JB, Olf HG, Peterlin A (1966) J Polym Sci A 4:941
23. Nakagawa H, Ishida Y (1973) J Polym Sci Polym Phys 11:2153
24. He Y, Fan Z, Hu Y, Wu T, Wei J, Li S (2007) Eur Polym J 4:431